

## Article

# Response of Hydrodynamic Characteristics to Tillage-Induced Microtopography of Rill Erosion Processes under Heavy Rainfalls

Shuqin He <sup>1,†</sup>, Jian Luo <sup>2,3,†</sup>, Zicheng Zheng <sup>2,\*</sup>, Wenfeng Ding <sup>4</sup> and Jigen Liu <sup>4</sup>

<sup>1</sup> College of Forestry, Sichuan Agricultural University, Chengdu 611130, China; hesq@sicau.edu.cn

<sup>2</sup> College of Resources Science, Sichuan Agricultural University, Chengdu 611130, China; jian.luo@im.u.edu.cn

<sup>3</sup> Inner Mongolia Key Laboratory of River and Lake Ecology, School of Ecology and Environment, Inner Mongolia University, Hohhot 010021, China

<sup>4</sup> Key Laboratory of River and Lake Control and Flood Control of the Middle and Lower Reaches of the Yangtze River, Ministry of Water Resources, Wuhan 430010, China; dingwf@mail.crsri.cn (W.D.); liujg@mail.crsri.cn (J.L.)

\* Correspondence: zichengzheng@sicau.edu.cn; Tel.: +86-28-86290986

† These authors contributed equally to this work.

**Abstract:** The occurrence and development of rill erosion depends on the hydraulic characteristics of water flow and underlying soil surface features. Our experiments include one-rainfall-intensity treatments ( $2.0 \text{ mm min}^{-1}$ ) and various microtopographic levels based on different tillage practices with smooth slope (CK), artificial digging (AD), and ridge tillage (RT) on a  $15^\circ$  slope. The results indicate the following: (1) The soil roughness index values were in the order of CK < AD < RT, and the spatial variability of different tillage practices had strong autocorrelations during different rill erosive stages. The codomain values decreased with the increase in microtopography. (2) The multifractal dimension values of tillage practices in various erosive stages were in the order of RT > AD > CT. The microtopography of different tilled slopes showed strong multifractal characteristics, and the multifractal characteristics were stronger as the microrelief heterogeneity increased. For the CK slope, the generalized fractal dimension span ( $\Delta D$ ) ranged between 0.0019 and 0.0058. For the AD slope,  $\Delta D$  was between 0.2901 and 0.5112. And, for the RT slope,  $\Delta D$  was between 0.4235 and 0.7626. (3) With the evolution of rill erosion, the flow pattern on different tilled slopes changed from subcritical transition flow to supercritical transition flow. (4) Soil roughness index and  $\Delta D$  had good correlations with hydrodynamic parameters. The stronger the erosive energy of runoff was, the higher the spatial heterogeneity of microtopography was. This study is expected to provide a theoretical basis for revealing the hydrodynamic mechanism of rill erosion in slope farmland.

**Keywords:** rill erosion; microtopography; hydrodynamics; purple soil areas



Citation: He, S.; Luo, J.; Zheng, Z.; Ding, W.; Liu, J. Response of Hydrodynamic Characteristics to Tillage-Induced Microtopography of Rill Erosion Processes under Heavy Rainfalls. *Land* **2024**, *13*, 685. <https://doi.org/10.3390/land13050685>

Academic Editor: Adrianos Retalis

Received: 6 April 2024

Revised: 8 May 2024

Accepted: 9 May 2024

Published: 14 May 2024



Copyright: © 2024 by the authors. Licensee MDPI, Basel, Switzerland. This article is an open access article distributed under the terms and conditions of the Creative Commons Attribution (CC BY) license (<https://creativecommons.org/licenses/by/4.0/>).

## 1. Introduction

Surface microtopography plays an important role in rainfall, runoff, and erosion processes [1]. Microtopography changes the flow convergence through its own changes in the relative height of space points, accompanied by water erosion, thus affecting water erosion evolution and sediment volume [2]. In contrast, water storage and sediment transport also affect the spatial distribution of microtopography [3]. Because of the complex and random nature of microtopography changes in the process of water erosion, its quantitative characterization has always been a hot issue in soil erosion science [4,5]. Surface microtopography is a result of the interplay among the orientation, periodic structure, and random fluctuations in three-dimensional space. One widely used approach for characterizing surface microtopography is to capture the fundamental structure of the soil surface by using a single index. The first is the random roughness value, which represents the

random distribution of surface microtopography by calculating the elevation standard deviation after removing the slope and tillage traces. According to Gómez et al. (2005), the initial state of random roughness can affect both runoff and sediment yield [6]. Meanwhile, Magunda et al. (1997) discovered that random roughness is inversely related to sediment yield [7]. However, the limitation of the random roughness index is its inability to consider the spatial characteristics of microtopography, focusing solely on the vertical component [8]. Another way to express microtopography is using geostatistical techniques, such as semivariograms [9]. A semivariogram can reflect the relationship between the elevation differences and the length scales, given by the separation lag [10]. Multifractal models have found wide-ranging applications in analyzing the scale-invariant characteristics of objects across various fields. Scale invariance has gained significance in comprehending the intricacy of natural phenomena [11], thereby highlighting the need for multifractal analysis as a valuable tool to address the nonlinear and complex challenges of geomorphic systems [2,12,13].

Rill erosion is a prevalent form of erosion that occurs on farmland, serving as the primary source of sediment and accounting for 50~90% of the total eroded sediment on sloping farmland [14–16]. The rill erosion process affects the change in surface microtopography on hillslopes [17], and conversely, microrelief plays a crucial role in shaping rills [18,19]. Due to the influence of rainfall, slope, soil texture, and other factors, the evolution of rill erosion on slope surface is complicated and has significant spatio-temporal variation [20]. At the same time, the rill erosion process affects the change in surface microtopography evolution, which has geomorphological significance [4,20]. Some researchers have indicated that rill erosion not only intensifies surface microtopography but also enhances the complexity of the spatial distribution of microtopography [21,22]. However, other studies have shown that changes in surface microtopography are negatively correlated with rill morphology parameters in various experimental scenarios [23].

Stream power, unit stream power, shear stress, and unit energy of cross section are basic hydrodynamic parameters to characterize the critical conditions of the water erosion process [22,24–26]. Purple soil formed from the purple rock series of the Jurassic and Cretaceous system and is mainly found in Sichuan Province, which is the most important agricultural area in southwest China. However, intensive cultivation and socioeconomic pressures have accelerated soil erosion on sloping farmlands [27]. Tillage-induced microtopography could not only efficiently control soil loss but also greatly intercept runoff on slopes [28]; however, tillage-induced microtopography increases soil erosion in the rill flow erosion process on the Loess Plateau [29]. The difference in these results may be related to the hydrodynamic characteristics of different soil surfaces in the evolution of water erosion. Although the hydrodynamic study of soil erosion has attracted much attention in recent years, the hydrodynamic characteristics and mechanism associated with different microrelief features and with the evolution of rill erosion remain ambiguous and necessitate further investigation. The objectives of this study are (1) to investigate the spatial variation characteristics of microtopography in the different stages of rill erosion, (2) to analyze the change in hydrodynamic parameters during the process of rill erosion, and (3) to clarify the relationship between microtopography changes and hydrodynamics during rill erosion.

## 2. Materials and Methods

### 2.1. Soil Sampling

Experimental samples were collected from the topsoil (0–20 cm) on a farm plot at the Ziyang Key Field Scientific Observation Station of Agricultural Resources and Ecological Environment in the Upper Reaches of Yangtze River, Ministry of Agriculture, China (104°34' E, 30°05' N). Soil was classified as purple soil that derived from Entisols [30]. The soil bulk density was  $1.20 \text{ g cm}^{-3}$ ; the soil organic matter content was  $13.0 \text{ g kg}^{-1}$ ; and the fractions of sand, silt, and clay were 49%, 29%, and 22%, respectively, based on the international system. Soil samples were air-dried naturally and passed through a 10 mm sieve to remove weeds and rocks and ensure homogeneity before the experiments.

## 2.2. Experimental Design

The experiments were conducted in an artificial rainfall field at the Key Laboratory of Soil and Water Conservation and Desertification Control, Sichuan Agricultural University. The sieved soil was placed in stainless steel soil flumes with adjustable slope gradients. The flumes were 4.0 m long, 0.8 m wide, and 0.5 m deep. Before filling the flumes with the sample soils, we first filled the flumes' base with a 5 cm thick layer of fine sand so that the permeability of the experimental soil layer was similar to that in the field. We then filled the flumes with a 10 cm soil layer individually. The layer was subsequently compacted to a bulk density of  $1.2 \text{ g cm}^{-3}$ , and the quantity of soil in each layer remained as consistent as feasible [25]. Soil moisture content of experimental soil was approximately 5% prior to the onset of rainfall events.

These three tillage practices were widely used in the hilly region of the Sichuan basin for agricultural production in sloping farmland. The experiment simulated different microrelief features based on different tillage practices. These tillage practices are typical in slope farmland in purple soil areas and mainly include smooth slope (CK), artificial digging (AD), and ridge tillage (RT) (Figure 1). CK was used to simulate smooth surface. AD was used to simulate moderate roughness, where the depth of the depression was 7 cm and the distance between the depressions was 25 cm. RT, representing a ridge–furrow system, was used to simulate roughness, where the ridges were 15 cm in height with a between-ridge distance of 80 cm. Based on the distribution of sloping farmland in the study area, soil flumes were tilted at an angle of  $15^\circ$ . The simulated rainfall experiments were conducted with a rainfall intensity of  $2.0 \text{ mm min}^{-1}$ , as per the characteristics of local storms that primarily occur during the summer and autumn seasons in the study area. The height of the rainfall simulator was 7 m above the ground, and detailed description about the rainfall simulator was presented by Luo et al. (2017) [2]. The rainfall durations for all the treatments were 90 min. The rill process can be divided into the four stages of drop-pit development stage (DP), intermittent rill stage (IR), rill development stage (RD) and rill stabilization stage (RS) [31].

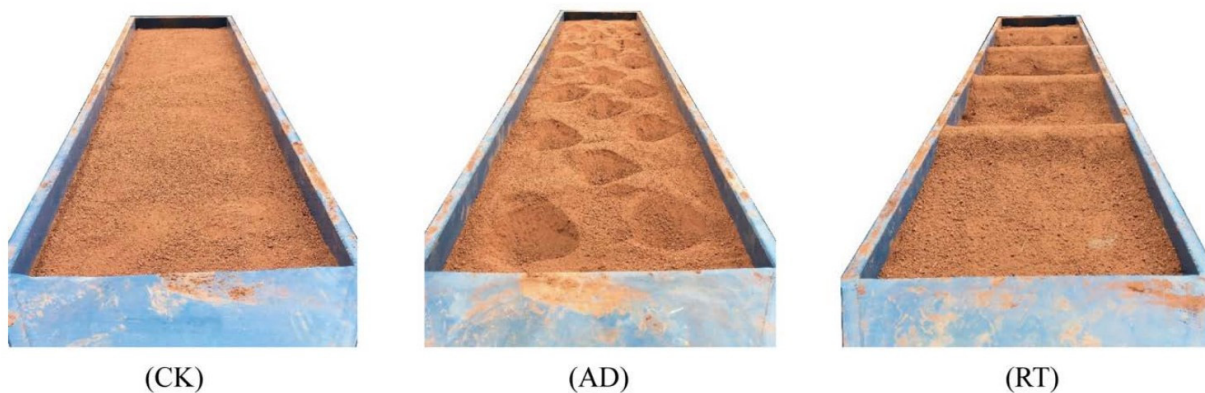


**Figure 1.** Layouts of the three tillage practices. CK: smooth slope; AD: artificial digging; RT: ridge tillage.

## 2.3. Digital Elevation Model Generation

The elevation information of microtopography caused by tillage was captured by using a laser scanner (MAPTEK I-Site 8820, Glenside, Australia) with a spatial resolution of  $1 \text{ mm} \times 1 \text{ mm}$  at the beginning and end of each rill erosive stage. We subjected the collected data to a series of pre-processing procedures (including denoising, spatial alignment, and coordinate transformation) by using MAPTEK I-Site studio software (2.0). The elevation point cloud data generated from the scanner were then converted to .txt format with xyz coordinates. The digital elevation models (DEMs) of microtopography caused by tillage were established by the method of kriging interpolation based on the ArcGIS 3D analyst model in ArcGIS software (10.8).

## 2.4. Collection of Runoff and Sediment Yield

Sediment and runoff were sampled at the flume outlet. The sample interval was 3 min for every experiment. All runoff samples were measured, oven-dried, and subsequently weighed to determine the sediment yield [32]. All experiments were repeated twice.

## 2.5. Data Calculation and Analysis

### (1) Soil roughness

The soil roughness index (SR) was calculated using the following formula [33]:

$$SR = 100 \times \log S \quad (1)$$

where  $S$  is the standard deviation of all the surface elevations.

### (2) Fractal analysis of microtopography

The fractal dimension of microtopography was determined based on the box-counting method [34,35]. The partition function ( $\mu_i(q, \varepsilon)$ ) can be obtained from the weighted summation of the  $q$ -th power of the elevation distribution probability.

$$\mu_i(q, \varepsilon) = \sum_{i=1}^{n(\varepsilon)} \mu_i(\varepsilon)^q \quad (2)$$

where  $q$  is the weight factor and the  $q$  values range from  $-3$  to  $+3$  with increments of  $0.5$ ;  $\varepsilon$  is size of the box and the box sizes were  $10, 30, 60, 90\dots 270$ , and  $300$  mm;  $\mu_i(\varepsilon)$  is the elevation distribution probability of the  $i$ -th subarea; and  $n(\varepsilon)$  is the number of boxes in which  $\mu_i(\varepsilon) > 0$ .

The fractal information dimension can be defined by

$$D(q) = \frac{1}{q-1} \lim_{\varepsilon \rightarrow 0} \frac{\ln \sum_{i=1}^{n(\varepsilon)} \mu_i(q, \varepsilon)}{\ln(\varepsilon)}, q \neq 1 \quad (3)$$

$$D_i = \lim_{\varepsilon \rightarrow 0} \frac{\sum_{i=1}^{n(\varepsilon)} \mu_i(\varepsilon) \ln \mu_i(\varepsilon)}{\ln(\varepsilon)}, q = 1 \quad (4)$$

where  $D(q)$  is the general fractal dimension and  $D_i$  is the fractal information dimension.

### (3) Semivariogram analysis

The semivariogram model (SM) is used to assess the spatial variation structure characteristics of microtopography. The SM is defined as

$$\gamma(h) = \frac{1}{2N(h)} \sum_{i=1}^{N(h)} [Z(x_i) - Z(x_i + h)]^2 \quad (5)$$

where  $\gamma(h)$  is the semivariance for the lag distance between sampling elevation data points ( $h$ ),  $Z(x_i)$  is the relative elevation at location  $x_i$ , and  $N(h)$  is the number of data pairs for lag distance  $h$ .

### (4) Rill flow hydraulic and hydrodynamic parameters

During the rainfall process, the velocity and depth of the rill flow were measured in three sections along the slope (1.5, 2.5, and 3.5 m) of the experimental plot. To determine the flow velocity, KMnO<sub>4</sub> was used as a tracer. The flow depth was measured vertically on

the upper, middle, and lower slopes by using a thin ruler with a precision of 0.1 mm. The Reynolds number ( $R_e$ ) was calculated as follows [36]:

$$Re = \frac{uR}{v_0} \quad (6)$$

$$v_0 = \frac{0.01775 \times 10^{-4}}{1 + 0.0337t + 0.00022t^2} \quad (7)$$

where  $u$  is the average flow velocity ( $\text{m s}^{-1}$ ),  $R$  is the hydraulic radius (m),  $v_0$  is the kinematic viscosity ( $\text{m}^2 \text{s}^{-1}$ ), and  $t$  is the temperature ( $^\circ\text{C}$ ).

The Froude number ( $Fr$ ) was calculated as follows [37]:

$$Fr = \frac{u}{\sqrt{gR}} \quad (8)$$

where  $g$  is gravitational acceleration ( $\text{m s}^{-2}$ ).

Manning's roughness ( $n$ ) was calculated as follows [38]:

$$n = \frac{R^{\frac{2}{3}}J^{\frac{1}{2}}}{u} \quad (9)$$

where  $J$  is the surface slope ( $\text{m m}^{-1}$ ).

The Darcy–Weisbach resistance coefficient ( $f$ ), the flow shear stress ( $\tau$ ), and the stream power ( $\omega$ ) were calculated by Equations (10)–(12), respectively [39]:

$$f = \frac{8gRJ}{u^2} \quad (10)$$

$$\tau = \gamma R J \quad (11)$$

$$\omega = \gamma q J \quad (12)$$

where  $\gamma$  is the weight density of water ( $\text{N m}^{-3}$ ) and  $q$  is the discharge per unit width ( $\text{m}^3 \text{s}^{-1}$ ).

The unit energy of the water-carrying section ( $E$ ) was calculated as follows [22]:

$$E = (\alpha u^2 / 2g) + h \quad (13)$$

where  $\alpha$  is a correction coefficient for kinetic energy, set to 1 in this study.

### 3. Results and Discussion

#### 3.1. Microtopography Dynamics during Rill Erosive Stages

Microtopography typically pertains to the soil surface's shape and contour, which are influenced by soil particles, aggregates, clods, and tillage operations, resulting in a relative elevation shift of 5~25 cm [5,40]. Given the complex and uncertain nature of microtopography in water erosion, there has been considerable interest among scholars in characterizing it qualitatively and quantitatively. Surface roughness (SR) is a widely used measure of microtopography. According to Figure 2, the tillage practices had SR index values in the order of CK < AD < RT for the different rill erosive stages.

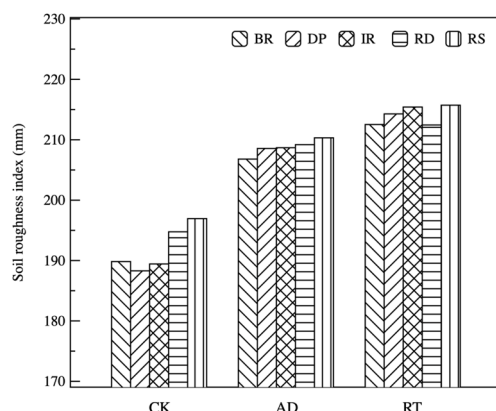


**Figure 2.** Change characteristics of soil roughness values on tilled slopes during rill erosive stages. CK: smooth slope; AD: artificial digging; RT: ridge tillage. BR: before-rainfall stage; DP: drop-pit development stage; IR: intermittent rill stage; RD: rill development stage; RS: rill stabilization stage.

For the CK slope, the SR index initially decreased and then increased with the evolution of rill erosion. In the DP, IR, RD, and RS stages, the SR index of the CK slope increased by 2.8%, 1.1%, 0.6%, and −0.8%, respectively. The reduction in SR index in the early stage of rainfall may be attributed to the compaction of loose soil particles by raindrops, which decreased the spatial heterogeneity of microtopography. As rills formed, the SR index increased gradually. For the AD slope, the SR index increased by 0.8%, 0.06%, 0.2%, and 0.5% in the DP, IR, RD, and RS stages, respectively. This result is consistent with the previous studies [4]. The SR index of the RT slope exhibited an increasing trend with the evolution of rill erosion, with increments of 0.8%, 0.5%, −1.4%, and 1.5% in the DP, IR, RD, and RS stages, respectively.

According to Zhang et al. [22], investigating the spatial distribution and heterogeneity of surface microtopography in the process of water erosion requires addressing three key questions: (1) What causes changes in surface microtopography in response to changes in surface roughness? (2) Which factors are the primary drivers of spatial variation in surface microtopography? (3) What specific spatial factors correspond to particular scales? Geostatistics is an effective means to deal with the above problems. Bullard et al. [41] showed that the spatial heterogeneity of surface microtopography was mainly affected by both structural factors and random factors based on the semivariogram method. According to Figure 3, it can be observed that the nugget values for different tillage practices increased with the evolution of rill erosion.

Additionally, the sill values of different tillage practices also increased with the increase in nugget values. The order of sill values for the tillage practices was RT > AD > CK. Moreover, the base effect values for all tillage practices were more than 75%, indicating strong or medium autocorrelations of spatial variability in surface microtopography during different stages of water erosion. This further implies that structural factors primarily contribute to the spatial heterogeneity of surface microtopography. The influence of tillage practice on the spatial heterogeneity of surface microtopography was far greater than that of other factors, which was consistent with the results of Zhang et al. [22]. The codomain values for each slope in different rill erosive stages are presented in Figure 2. Specifically, for the CK slope, the codomain values were 3.87, 3.93, 3.63, 3.31, and 3.27 m in the BR, DP, IR, RD, and RS stages, respectively. For the AD slope, the codomain values were 3.10, 2.90, 2.70, 2.40, and 1.93 m in the BR, DP, IR, RD, and RS stages, respectively. For the RT slope, the codomain values were 1.67, 1.51, 1.42, 1.28, and 1.20 m in the BR, DP, IR, RD, and RS stages, respectively. In general, the codomain values decreased as the micrelief heterogeneity increased.

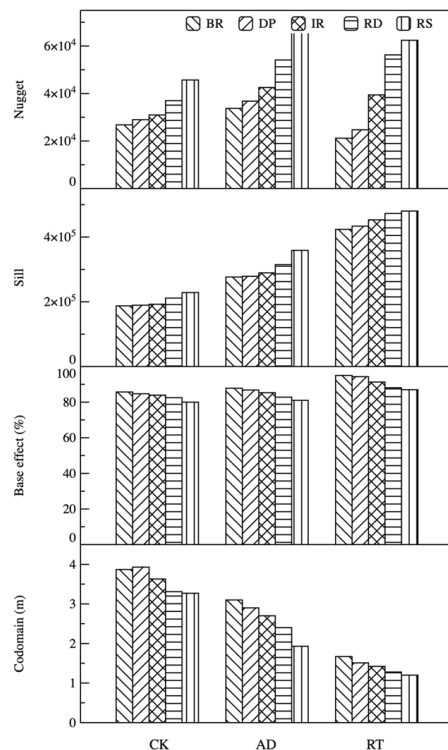


**Figure 3.** Parameters of the semivariogram models on tilled slopes in different erosive stages. CK: smooth slope; AD: artificial digging; RT: ridge tillage. BR: before-rainfall stage; DP: drop-pit development stage; IR: intermittent rill stage; RD: rill development stage; RS: rill stabilization stage.

Multifractal refers to complex objects composed of multiple simple fractals in space, which allows for the analysis of scale invariance. The concept of scale invariance is of growing interest in understanding the complexity of natural phenomena, and multifractals have found wide application in the geosciences. For example, based on fractal theory, Manninen [12] demonstrated the multiscale behavior of bare land, while Roisin [13] established the effectiveness of multifractal analysis in evaluating the internal heterogeneity of cultivated soil. Luo et al. [2] depicted the structural characteristics of soil surface microtopography in the process of water erosion evolution by using spectral functions. Figure 4 shows that the  $D_q$  of different slopes decreased monotonically with the increase in  $q$  with the evolution of rill erosion.

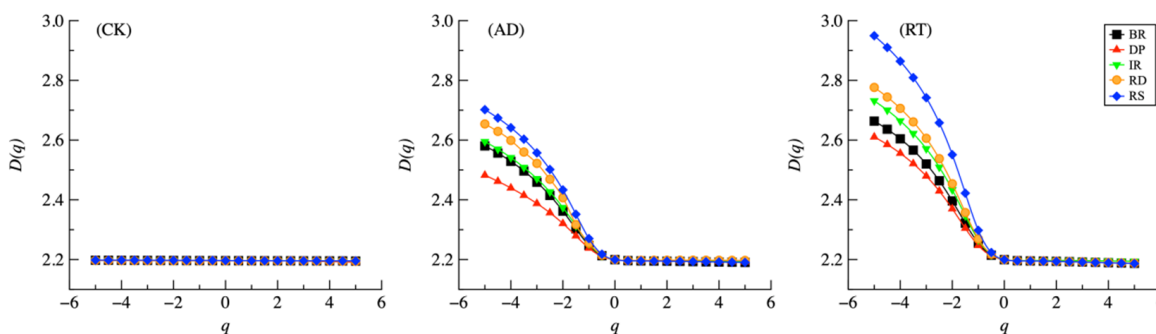


**Figure 4.** Change characteristics of the generalized fractal dimension on tilled slopes in different rill erosive stages. CK: linear slope; AD: artificial digging; RT: ridge tillage. BR: before-rainfall stage; DP: drop-pit development stage; IR: intermittent rill stage; RD: rill development stage; RS: rill stabilization stage.

For the CK slope, the generalized dimension spectra  $D_q \sim q$  could be described by a linear curve, while the generalized dimension spectra  $D_q \sim q$  of the AD and RT slopes

displayed S-shaped curves. When the weight factor ( $q$ ) is 0, 1, and 2, the corresponding generalized fractal dimension  $D$  ( $q$ ) is called capacity dimension ( $D_0$ ), information dimension ( $D_1$ ), and correlation dimension ( $D_2$ ), respectively. Generally speaking, if  $D(q)$  remains constant, the object behaves as a single fractal; if  $D_0 = D_1 = D_2$ , the object shows complete self-similarity; if  $D_0 > D_1 > D_2$ , the object shows multifractal characteristics [42]. For the CK slope,  $D_0$ ,  $D_1$ , and  $D_2$  were 2.1962, 2.1960, and 2.1956, respectively. For the AD slope,  $D_0$ ,  $D_1$ , and  $D_2$  were 2.1996, 2.1968, and 2.1962, respectively. And, for the RT slope,  $D_0$ ,  $D_1$ , and  $D_2$  were 2.1996, 2.1954, and 2.1941, respectively. In general, the surface microtopography of the tilled slopes exhibited a significant degree of multifractality, with stronger multifractal characteristics observed as the microrelief heterogeneity increased.  $\Delta D(D_{\max} - D_{\min})$  can quantify the degree of disorder of spatial distribution of surface microtopography. The larger  $\Delta D$  is, the higher the spatial heterogeneity of surface microtopography is [43]. For the CK slope,  $\Delta D$  ranged between 0.0019 and 0.0058. For the AD slope,  $\Delta D$  was between 0.2901 and 0.5112. And, for the RT slope,  $\Delta D$  was between 0.4235 and 0.7626. Tillage practices increase the spatial heterogeneity of soil microtopography, and this could result in a more complex relationship between tillage and soil erosion [4,29].

### 3.2. Changes in Flow Hydraulics during Rill Erosive Stages

Soil erosion is mainly driven by runoff, with rill erosion being one of the most severe forms of water erosion on slopes [29,44]. As such, studying the hydrodynamic characteristics of rill flow has great theoretical value in understanding the mechanism of rill erosion [45]. Figure 5 shows the spatial distribution of runoff velocity on the CK slope in various rill erosive stages.

The slope surface was divided into three sections from the bottom to the top of the flume, and the average runoff velocity of inter-rill areas in each section and the rill flow velocity at key locations were marked in Figure 5. The trend of runoff velocity in the inter-rill areas remained consistent across different erosive stages, with velocities gradually increasing from the upper to the lower slopes. This is mainly because with the increase in slope length, the catchment area above the slope increased, and the corresponding flow energy increased accordingly [43,44]. The velocity of rill flow varied with the morphology of the rill as it developed. During the rill formation stage, the rill flow velocity was relatively high compared with the runoff velocity in the inter-rill areas, due to the large amount of runoff from inter-rill areas flowing into the rills, which increased the runoff energy. However, as rill erosion progressed, the rill flow velocity gradually decreased. This was mainly because the continuous development of rills resulted in increased rill density and resistance of the rill bed, which weakened the runoff energy and hydrological connectivity, ultimately reducing the flow velocity of the rills [15]. In addition, the response of surface microtopography to soil erosion varies with changes in hydrological sediment connectivity [46], and the formation of rills results in increased hydrological sediment connectivity on tilled slopes; therefore, flow velocity increases with the evolution of water erosion [47].

For the AD slope, the runoff velocity from the upper slope to the lower slope showed a gradually increasing trend. The runoff velocity at different slope positions was relatively small compared with the CK slope. The RT slope initially exhibited relatively low runoff velocity before ridge collapse. With the evolution of rill erosion, the runoff connectivity was constantly enhanced, resulting in an increase in the runoff velocity at different positions on the slope. Reichert and Norton (2013) showed that rill flow has transitional flow and turbulent flow characteristics [48]. Figure 6A shows the variation characteristics of the Reynolds number ( $Re$ ) of each tilled slope during rainfall. According to open-channel flow theory, we have laminar flow when  $Re < 500$ , we have transitional flow when  $500 < Re < 5000$ , and we have turbulent flow when  $Re > 5000$ . The graph in Figure 6B illustrates the changes in Froude number ( $Fr$ ) for each tilled slope during the rainfall event.

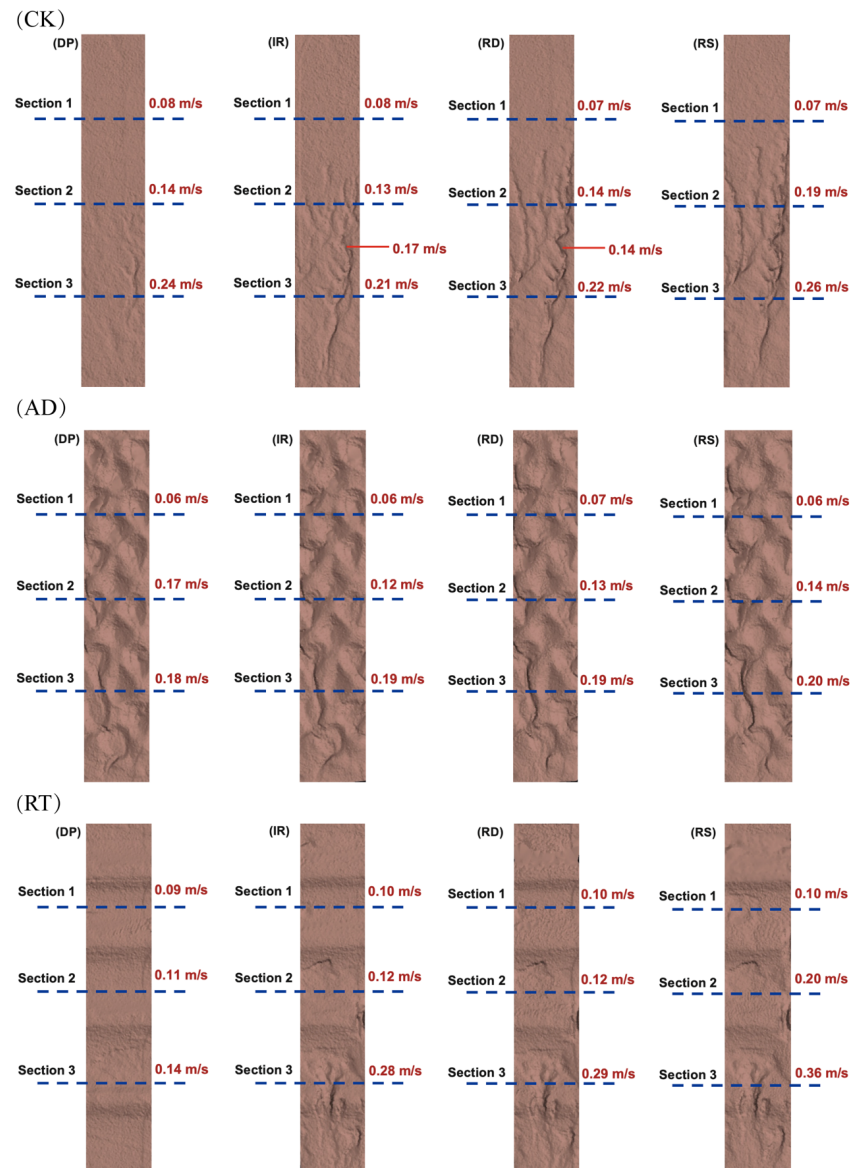


**Figure 5.** Spatial distribution of flow velocity on tilled slopes during different rill erosive stages. CK: smooth slope; AD: artificial digging; RT: ridge tillage. DP: drop-pit development stage; IR: intermittent rill stage; RD: rill development stage; RS: rill stabilization stage.

In the log–log plots of runoff velocity and hydraulic radius, three boundary lines ( $Re = 500$ ,  $Re = 5000$ , and  $Fr = 1$ ) were drawn to separate sheet flow and rill flow into six flow regimes (Figure 7). Figure 7 illustrates how the flow pattern on different tilled slopes changed from subcritical transition flow to supercritical transition flow with the evolution of soil erosion. When  $Fr < 1$ , flow is considered subcritical, while flow is considered supercritical when  $Fr > 1$ . The results show that the Froude numbers varied among the different tilled slopes, but all remained below 1, indicating that all flows were classified as subcritical flow. The subcritical laminar flow class is defined as  $Re < 500$  and  $Fr < 1$ . The subcritical transition flow class is defined as  $500 < Re < 5000$  and  $Fr < 1$ . The subcritical turbulent flow class is defined as  $Re > 5000$  and  $Fr < 1$ . The supercritical laminar flow class is defined as  $Re < 500$  and  $Fr > 1$ . The supercritical transition flow class is defined as  $500 < Re < 5000$  and  $Fr > 1$ . The supercritical turbulent flow class is defined as  $Re > 5000$  and  $Fr > 1$ . The Reynolds number of different tilled slope showed a trend of increasing gradually with the evolution of soil erosion, with some  $Re$  exceeding 5000 and entering the category of turbulent flow. However, the Froude number was less than 1 under different

conditions, indicating that the microtopographic-scale flow belonged to the category of slow flow in our study.

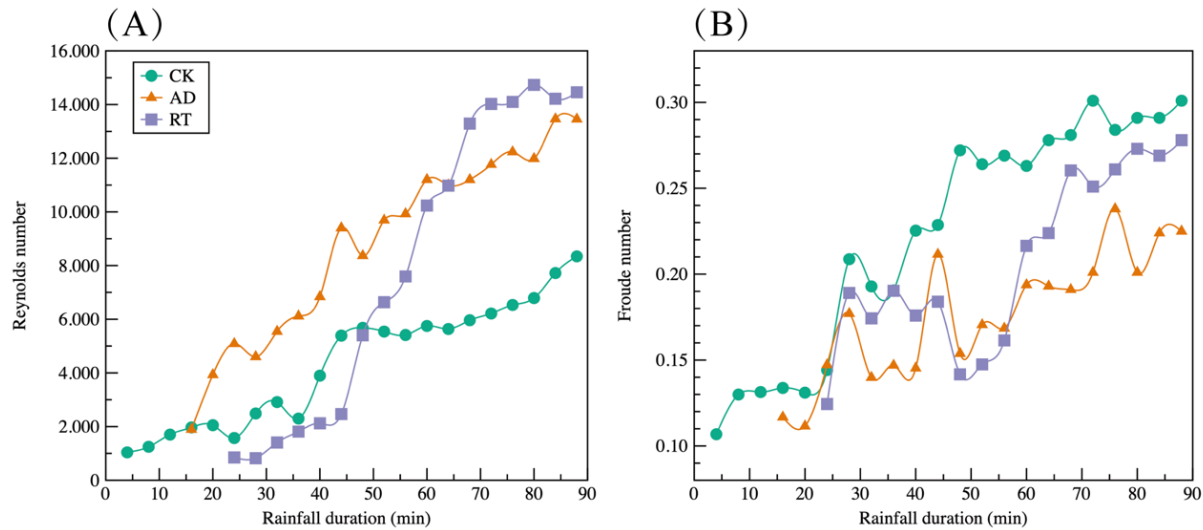


**Figure 6.** Change characteristics of Reynolds number (A) and Froude number (B) for tilled slopes during rainfall. CK: smooth slope; AD: artificial digging; RT: ridge tillage.

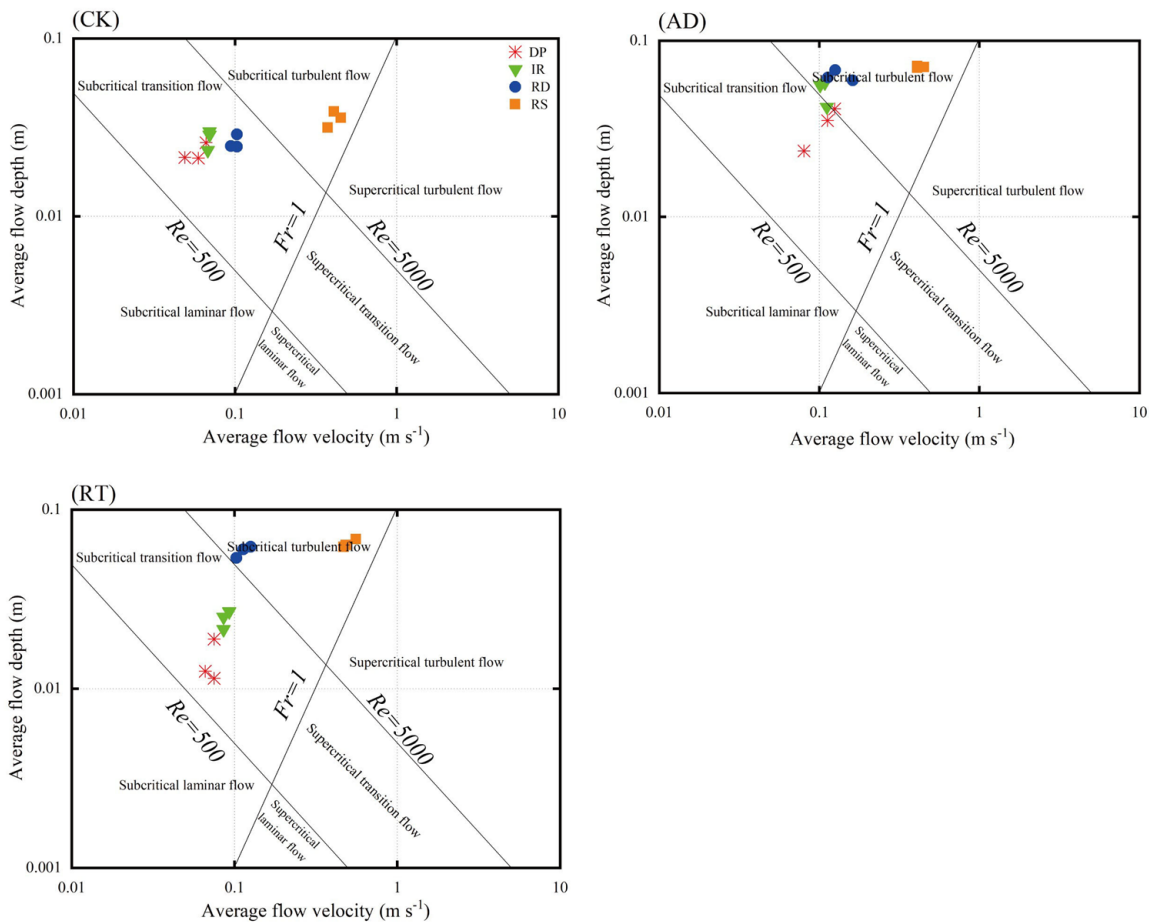


**Figure 7.** Flow state zoning of rills on tilled slopes in different rill erosive stages. CK: smooth slope; AD: artificial digging; RT: ridge tillage. DP: drop-pit development stage; IR: intermittent rill stage; RD: rill development stage; RS: rill stabilization stage.

Specifically, for the CK slope, rill flow in the DP, IR, and RD stages was subcritical transition flow, while in the RS stage, it was supercritical transition flow. Similarly, in the AD slope, rill flow in the DP stage was subcritical transition flow, while in the IR, RD, and RS stages, it was supercritical transition flow. On the RT slope, rill flow in the DP and IR stages was subcritical transition flow, while in the RD and RS stages, it was supercritical transition flow. The results showed that the evolution of rill erosion changed the hydrodynamic characteristics of runoff, and microtopographic factors accelerated the transformation process of the flow regime. During the occurrence and development of rill erosion on the slope, the rill flow is inevitably subject to flow resistance. The trend of the Darcy–Weisbach resistance coefficient during rainfall is illustrated in Figure 8.

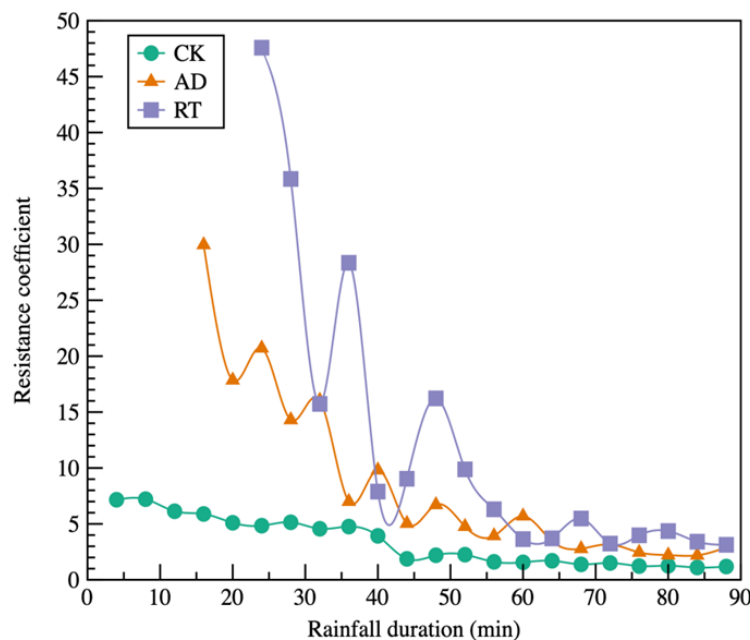


**Figure 8.** Change characteristics of Darcy–Weisbach resistance coefficient on tilled slopes during rainfall. CK: smooth slope; AD: artificial digging; RT: ridge tillage.

For the CK slope, the resistance coefficient decreased gradually. However, the AD and RT slopes showed a fluctuating decreasing trend. In terms of the overall resistance coefficient, the RT slope exhibited the highest value, followed by the AD slope, and then the CK slope. This may be related to the fluctuation in surface microtopography caused by different tillage practices, and it was found that the RT and AD slopes may have had obvious fluctuations in the process of rainfall due to the interaction between slope erosion evolution and surface microtopography. Soil erosion is an energy-consuming process [49]. Many scholars have performed a lot of research on the dynamic mechanism of slope erosion [50,51], but the results are not consistent. These differences in results may be related to soil properties and experimental conditions. In particular, which dynamic parameters can accurately characterize the rill development mechanism of surface microtopography needs to be further discussed. In this study, the hydrodynamic parameters, including flow shear stress, stream power, unit stream power, and unit energy of the water-carrying section, increased with the increase in rainfall duration on the tilled slopes, as shown in Figure 9. The CK slope showed a relatively stable change in hydrodynamic parameters during rill erosion. However, the AD and RT slopes showed significant fluctuations, especially during the IR stage. The rill development with time and space affects the hydraulic characteristics of overland flow [52]. Meanwhile, the dynamic change in overland flow inevitably leads to the further development of rill morphology [53].

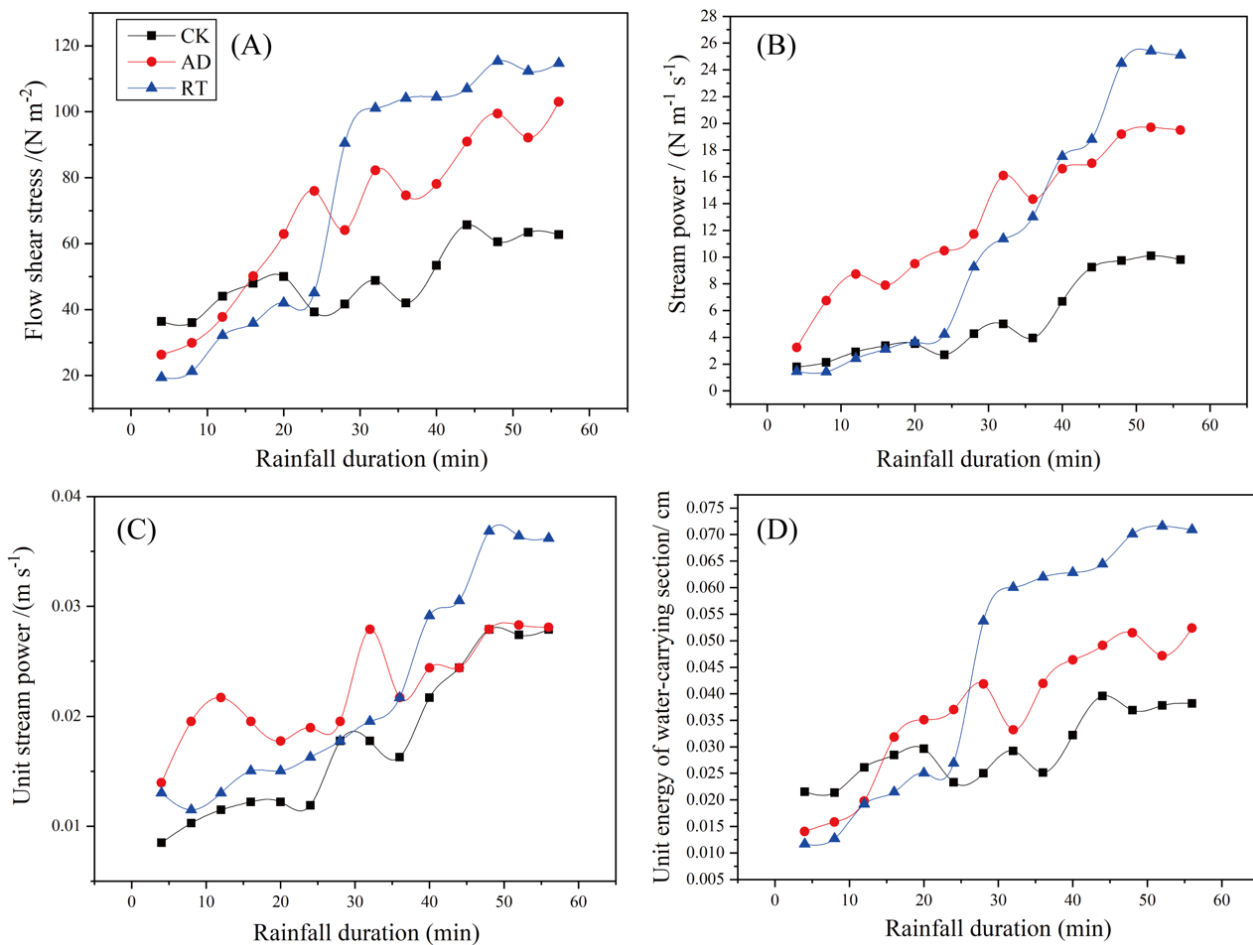


**Figure 9.** Change characteristics of hydrodynamic parameters ((A) flow shear stress; (B) stream power; (C) unit stream power; (D) unit energy of water-carrying section) of tilled slopes during rainfall. CK: smooth slope; AD: artificial digging; RT: ridge tillage.

### 3.3. Response of Hydrodynamic Characteristics to Soil Surface Microtopography

The correlation between microtopography and hydrodynamic parameters was further elucidated by incorporating various tillage practices and erosive stages. Table 1 shows the relationship between microtopographic parameters and rill flow hydraulic and hydrodynamic parameters. The SR value reflects the variation of microtopography in the vertical direction, and  $\Delta D$  reveals the spatial heterogeneity of microtopography [23]. The correlation analysis showed that the SR value had a strong correlation with  $\Delta D$ , which is consistent with the result of Zheng et al. [54]. Moreover, the hydrodynamic parameters were also strongly correlated with the SR value, with the correlation coefficients decreasing in the order of  $\varphi > \tau > E > \omega$ . Similarly,  $\Delta D$  exhibited significant correlations with the hydrodynamic parameters, and  $R^2$  ranged from 0.896 to 0.929. During rill erosion, runoff was the main driving force [55]. As sediment was transported and energy was exchanged, the rill morphology changed [53], which in turn affected the spatial heterogeneity of microtopography. Specifically, the stronger the erosive energy of runoff was, the higher the spatial heterogeneity of microtopography was. On the contrary, microtopography enhanced the hydrodynamic forces operating on the soil surface, which contributed to the increase in the sediment yield of the hillslope.

**Table 1.** Correlation matrix for microtopographic parameters and rill flow hydraulic and hydrodynamic parameters.

	<i>SR</i>	<i>ΔD</i>	<i>Re</i>	<i>Fr</i>	<i>f</i>	$\tau$	$\omega$	$\varphi$	<i>E</i>
<i>SR</i>	1								
<i>ΔD</i>	0.931 **	1							
<i>Re</i>	0.478	0.647	1						
<i>Fr</i>	0.343	0.198	0.345	1					
<i>f</i>	−0.512	−0.323	−0.351	−0.448	1				
$\tau$	0.859 **	0.896 **	0.461	0.326	−0.428	1			
$\omega$	0.818 **	0.912 **	0.549	0.297	−0.363	0.964 **	1		
$\varphi$	0.886 **	0.929 **	0.564	0.428	−0.496	0.953 **	0.970 **	1	
<i>E</i>	0.858 **	0.897 **	0.465	0.322	−0.424	0.966 **	0.966 **	0.953 **	1

Note: *SR*: soil roughness value; *ΔD*: generalized fractal dimension span; *Re*: Reynolds number; *Fr*: Froude number; *f*: Darcy–Weisbach resistance coefficient;  $\tau$ : shear stress;  $\omega$ : stream power;  $\varphi$ : unit stream power; *E*: unit energy of water-carrying section. \*\* means the correlation between two variables is significant at  $p < 0.01$ .

#### 4. Conclusions

Rainfall simulation experiments were conducted under high-intensity erosive rainfall events ( $2.0 \text{ mm min}^{-1}$ ) and high slope gradient ( $15^\circ$ ) to examine how the microtopography and hydrodynamic parameters dynamically changed as rill erosion evolved. The results indicate that the microtopography of different tilled slopes showed strong multifractal and autocorrelation characteristics during different rill erosive stages. Moreover, the strength of multifractal characteristics was positively associated with the extent of microrelief. The multifractal dimension values of tillage practices in various erosive stages were in the order of  $RT > AD > CT$ . With the evolution of soil erosion, the flow pattern on different tilled slopes changed from subcritical transition flow to supercritical transition flow. Strong correlations were found between microtopographic parameters and hydrodynamic parameters, indicating that runoff energy played a significant role in shaping the spatial heterogeneity of microtopography. Specifically, the study found that as the erosive energy of runoff increased, the spatial heterogeneity of microtopography became more pronounced. As a result, microtopography enhanced the hydrodynamic forces operating on the soil surface, which contributed to the increase in sediment yield. Therefore, the influence of surface microtopography on soil erosion and the interaction between erosion dynamics and surface microtopography should be fully considered during the allocation of tillage practices in future research.

**Author Contributions:** S.H.: conceptualization; investigation; methodology; project administration; resources; supervision; validation; writing—original draft; writing—review and editing. J.L. (Jian Luo): investigation; writing—original draft; methodology; validation; writing—review and editing. Z.Z.: conceptualization; investigation; methodology; project administration; supervision; validation; writing—review and editing. W.D. and J.L. (Jigen Liu): data curation; methodology; validation; visualization; project administration; writing—review. All authors have read and agreed to the published version of the manuscript.

**Funding:** This study was supported by the CRSRI Open Research Program, grant number CKWV20211870/KY, and National Natural Science Foundation of China, grant number 42177316.

**Data Availability Statement:** The raw data supporting the conclusions of this article will be made available by the authors on request.

**Conflicts of Interest:** The authors declare no conflicts of interest.

#### References

1. Zhao, L.S.; Huang, C.H.; Wu, F.Q. Effect of microrelief on water erosion and their changes during rainfall. *Earth Surf. Proc. Landf.* **2016**, *41*, 579–586. [[CrossRef](#)]
2. Luo, J.; Zheng, Z.C.; Li, T.X.; He, S.Q. Spatial heterogeneity of microtopography and its influence on the flow convergence of slopes under different rainfall patterns. *J. Hydrol.* **2017**, *545*, 88–99. [[CrossRef](#)]

3. Zhang, K.; Wang, G.; Sun, X.; Wang, J. Hydraulic characteristic of overland flow under different vegetation coverage. *Adv. Water Sci.* **2014**, *25*, 825–834, (In Chinese with English Abstract).
4. Luo, J.; Zheng, Z.; Li, T.; He, S. Assessing the impacts of microtopography on soil erosion under simulated rainfall, using a multifractal approach. *Hydrol. Process.* **2018**, *32*, 2543–2556. [[CrossRef](#)]
5. Vermang, J.; Norton, L.D.; Huang, C.; Cornelis, W.M.; Da Silva, A.M.; Gabriels, D. Characterization of soil surface roughness effects on runoff and soil erosion rates under simulated rainfall. *Soil Sci. Soc. Am. J.* **2015**, *79*, 903–916. [[CrossRef](#)]
6. Gómez, J.A.; Nearing, M.A. Runoff and sediment losses from rough and smooth soil surfaces in a laboratory experiment. *Catena* **2005**, *59*, 253–266. [[CrossRef](#)]
7. Magunda, M.K.; Larson, W.E.; Linden, D.R.; Nater, E.A. Changes in microrelief and their effects on infiltration and erosion during simulated rainfall. *Soil Technol.* **1997**, *10*, 57–67. [[CrossRef](#)]
8. Huang, C.H.; Bradford, J.M. Applications of a laser scanner to quantify soil microtopography. *Soil Sci. Soc. Am. J.* **1992**, *56*, 14–21. [[CrossRef](#)]
9. Dalla Rosa, J.; Cooper, M.; Darboux, F.; Medeiros, J.C. Soil roughness evolution in different tillage systems under simulated rainfall using a semivariogram-based index. *Soil Tillage Res.* **2012**, *124*, 226–232. [[CrossRef](#)]
10. Vázquez, E.V.; Vieira, S.R.; De Maria, I.C.; González, A.P. Fractal dimension and geostatistical parameters for soil microrelief as a function of cumulative precipitation. *Sci. Agric.* **2010**, *67*, 78–83. [[CrossRef](#)]
11. Moreno, R.G.; Alvarez, M.D.; Requejo, A.S.; Delfa, J.V.; Tarquis, A.M. Multiscaling analysis of soil roughness variability. *Geoderma* **2010**, *160*, 22–30. [[CrossRef](#)]
12. Manninen, A.T. Multiscale surface roughness description for scattering modelling of bare soil. *Physica A* **2003**, *319*, 535–551. [[CrossRef](#)]
13. Roisin, C.J. A multifractal approach for assessing the structural state of tilled soils. *Soil Sci. Soc. Am. J.* **2007**, *71*, 15–25. [[CrossRef](#)]
14. Kimaro, D.N.; Poesen, J.; Msanya, B.M.; Deckers, J.A. Magnitude of soil erosion on the northern slope of the Uluguru Mountains, Tanzania: Interrill and rill erosion. *Catena* **2008**, *75*, 38–44. [[CrossRef](#)]
15. Di Stefano, C.; Ferro, V.; Palmeri, V.; Pampalone, V. Measuring rill erosion using structure from motion: A plot experiment. *Catena* **2017**, *156*, 383–392. [[CrossRef](#)]
16. Jiang, Y.; Shi, H.; Wen, Z.; Guo, M.; Zhao, J.; Cao, X.; Zheng, C. The dynamic process of slope rill erosion analyzed with a digital close range photogrammetry observation system under laboratory conditions. *Geomorphology* **2020**, *350*, 106893. [[CrossRef](#)]
17. Kou, P.; Xu, Q.; Yunus, A.P.; Dong, X.; Zhong, Y.; Chen, L.; Jin, Z. Rill development and its change rate: A field experiment under constant rainfall intensity. *Catena* **2021**, *199*, 105112. [[CrossRef](#)]
18. Carollo, F.G.; Di Stefano, C.; Ferro, V.; Pampalone, V. Measuring rill erosion at plot scale by a drone-based technology. *Hydrol. Process.* **2015**, *29*, 3802–3811. [[CrossRef](#)]
19. Wu, S.; Chen, L.; Wang, N.; Yu, M.; Assouline, S. Modeling rainfall-runoff and soil erosion processes on hillslopes with complex rill network planform. *Water Resour. Res.* **2018**, *54*, 10–117. [[CrossRef](#)]
20. Berger, C.; Schulze, M.; Rieke-Zapp, D.; Schlunegger, F. Rill development and soil erosion: A laboratory study of slope and rainfall intensity. *Earth Surf. Proc. Landf.* **2010**, *35*, 1456–1467. [[CrossRef](#)]
21. Gómez, J.A.; Darboux, F.; Nearing, M.A. Development and evolution of rill networks under simulated rainfall. *Water Resour. Res.* **2003**, *39*, 1148. [[CrossRef](#)]
22. Zhang, L.T.; Gao, Z.L.; Yang, S.W.; Li, Y.H.; Tian, H.W. Dynamic processes of soil erosion by runoff on engineered landforms derived from expressway construction: A case study of typical steep spoil heap. *Catena* **2015**, *128*, 108–121. [[CrossRef](#)]
23. Luo, J.; Zheng, Z.; Li, T.; He, S. Spatial variation of microtopography and its effect on temporal evolution of soil erosion during different erosive stages. *Catena* **2020**, *190*, 104515. [[CrossRef](#)]
24. Nearing, M.A.; Norton, L.D.; Bulgakov, D.A.; Larionov, G.A.; West, L.T.; Dontsova, K.M. Hydraulics and erosion in eroding rills. *Water Resour. Res.* **1997**, *33*, 865–876. [[CrossRef](#)]
25. An, J.; Zheng, F.; Lu, J.; Li, G. Investigating the role of raindrop impact on hydrodynamic mechanism of soil erosion under simulated rainfall conditions. *Soil Sci.* **2012**, *177*, 517–526. [[CrossRef](#)]
26. McIsaac, G.F.; Mitchell, J.K.; Hummel, J.W.; Elliot, W.J. An evaluation of unit stream power theory for estimating soil detachment and sediment discharge from tilled soils. *Trans. ASABE* **1992**, *35*, 535–544. [[CrossRef](#)]
27. Yang, Y.; Ye, Z.H.; Liu, B.Y.; Zeng, X.Q.; Fu, S.H.; Lu, B.J. Nitrogen enrichment in runoff sediments as affected by soil texture in Beijing mountain area. *Environ. Monit. Assess.* **2014**, *186*, 971–978. [[CrossRef](#)] [[PubMed](#)]
28. da Rocha Junior, P.R.; Bhattacharai, R.; Alves Fernandes, R.B.; Kalita, P.K.; Vaz Andrade, F. Soil surface roughness under tillage practices and its consequences for water and sediment losses. *J. Soil Sci. Plant Nutr.* **2016**, *16*, 1065–1074. [[CrossRef](#)]
29. Zhao, L.; Hou, R.; Wu, F. Effect of tillage on soil erosion before and after rill development. *Land Degrad. Dev.* **2018**, *29*, 2506–2513. [[CrossRef](#)]
30. Soil Survey Staff. *Keys to Soil Taxonomy*, 11th ed.; USDA/NRCS: Washington, DC, USA, 2010.
31. Yan, D.C.; Wang, Y.F.; Wen, A.B.; Shi, Z.L.; Long, Y. Configuration evolvement of rill development on purple sloped land. *J. Mt. Sci.* **2011**, *29*, 469–473.
32. He, J.; Li, X.; Jia, L.; Gong, H.; Cai, Q. Experimental study of rill evolution processes and relationships between runoff and erosion on clay loam and loess. *Soil Sci. Soc. Am. J.* **2014**, *78*, 1716–1725. [[CrossRef](#)]
33. Kuipers, H. A reliefmeter for soil cultivation studies. *Neth. J. Agric. Sci.* **1957**, *5*, 255–262. [[CrossRef](#)]

34. Ferreiro, J.P.; Vázquez, E.V. Multifractal analysis of Hg pore size distributions in soils with contrasting structural stability. *Geoderma* **2010**, *160*, 64–73. [[CrossRef](#)]
35. Torre, I.G.; Losada, J.C.; Heck, R.J.; Tarquis, A.M. Multifractal analysis of 3D images of tillage soil. *Geoderma* **2018**, *311*, 167–174. [[CrossRef](#)]
36. Xu, X.; Zheng, F.; Wilson, G.V. Flow hydraulics in an ephemeral gully system under different slope gradients, rainfall intensities and inflow conditions. *Catena* **2021**, *203*, 105359. [[CrossRef](#)]
37. Pan, C.; Shangguan, Z.; Lei, T. Influences of grass and moss on runoff and sediment yield on sloped loess surfaces under simulated rainfall. *Hydrol. Process.* **2006**, *20*, 3815–3824. [[CrossRef](#)]
38. Li, T.; Liang, C.; Zhang, Y.; Zhao, P. Comparison and validation of the ratio of Manning coefficient to flow depth for soil erosion prediction using published data with different external impacts. *J. Soils Sediments* **2017**, *17*, 1682–1695. [[CrossRef](#)]
39. Xu, X.; Zheng, F.; Qin, C.; Wu, H.; Wilson, G.V. Impact of cornstalk buffer strip on hillslope soil erosion and its hydrodynamic understanding. *Catena* **2017**, *149*, 417–425. [[CrossRef](#)]
40. Zhu, P.; Zhang, G.; Wang, H.; Zhang, B.; Wang, X. Land surface roughness affected by vegetation restoration age and types on the Loess Plateau of China. *Geoderma* **2020**, *366*, 114240. [[CrossRef](#)]
41. Bullard, J.E.; Ockelford, A.; Strong, C.L.; Aubault, H. Impact of multi-day rainfall events on surface roughness and physical crusting of very fine soils. *Geoderma* **2018**, *313*, 181–192. [[CrossRef](#)]
42. Vidal Vázquez, E.; Miranda, J.G.V.; Paz-Ferreiro, J. A multifractal approach to characterize cumulative rainfall and tillage effects on soil surface micro-topography and to predict depression storage. *Biogeosciences* **2010**, *7*, 2989–3004. [[CrossRef](#)]
43. He, S.; Qin, F.; Zheng, Z.; Li, T. Changes of soil microrelief and its effect on soil erosion under different rainfall patterns in a laboratory experiment. *Catena* **2018**, *162*, 203–215. [[CrossRef](#)]
44. Zhang, P.; Yao, W.; Tang, H.; Wei, G.; Wang, L. Laboratory investigations of rill dynamics on soils of the Loess Plateau of China. *Geomorphology* **2010**, *293*, 201–210. [[CrossRef](#)]
45. Mirzaee, S.; Ghorbani-Dashtaki, S. Deriving and evaluating hydraulics and detachment models of rill erosion for some calcareous soils. *Catena* **2018**, *164*, 107–115. [[CrossRef](#)]
46. Luo, J.; Zheng, Z.C.; He, S.Q.; Ding, W.F. Multi-temporal spatial modelling to assess runoff and sediment dynamics under different microtopographic patterns. *Geoderma* **2023**, *436*, 116539. [[CrossRef](#)]
47. Luo, J.; Zheng, Z.C.; Li, T.X.; He, S.Q.; Tarolli, P. Impact of tillage-induced microtopography on hydrological-sediment connectivity and its hydrodynamic understanding. *Catena* **2023**, *228*, 107168. [[CrossRef](#)]
48. Reichert, J.M.; Norton, L.D. Rill and interrill erodibility and sediment characteristics of clayey Australian Vertosols and a Ferrosol. *Soil Res.* **2013**, *51*, 1–9. [[CrossRef](#)]
49. Jafarpoor, A.; Sadeghi, S.H.; Darki, B.Z.; Homaei, M. Changes in morphologic, hydraulic, and hydrodynamic properties of rill erosion due to surface inoculation of endemic soil cyanobacteria. *Catena* **2022**, *208*, 105782. [[CrossRef](#)]
50. Wang, D.; Wang, Z.; Shen, N.; Chen, H. Modeling soil detachment capacity by rill flow using hydraulic parameters. *J. Hydrol.* **2016**, *535*, 473–479. [[CrossRef](#)]
51. Xiao, H.; Liu, G.; Liu, P.; Zheng, F.; Zhang, J.; Hu, F. Response of soil detachment rate to the hydraulic parameters of concentrated flow on steep loessial slopes on the Loess Plateau of China. *Hydrol. Process.* **2017**, *31*, 2613–2621. [[CrossRef](#)]
52. Sun, J.; Zhang, N.; Shi, M.; Zhai, Y.; Wu, F. The effects of tillage induced surface roughness, slope and discharge rate on soil detachment by concentrated flow: An experimental study. *Hydrol. Process.* **2021**, *35*, e14261. [[CrossRef](#)]
53. Zhang, P.; Tang, H.; Yao, W.; Zhang, N.; Xizhi, L.V. Experimental investigation of morphological characteristics of rill evolution on loess slope. *Catena* **2016**, *137*, 536–544. [[CrossRef](#)]
54. Zheng, Z.C.; Qin, F.; Li, T.X. Changes in soil surface microrelief of purple soil under different slope gradients and its effects on soil erosion. *Trans. CSAE* **2015**, *31*, 168–175.
55. Tian, P.; Xu, X.; Pan, C.; Hsu, K.; Yang, T. Impacts of rainfall and inflow on rill formation and erosion processes on steep hillslopes. *J. Hydrol.* **2017**, *548*, 24–39. [[CrossRef](#)]

**Disclaimer/Publisher's Note:** The statements, opinions and data contained in all publications are solely those of the individual author(s) and contributor(s) and not of MDPI and/or the editor(s). MDPI and/or the editor(s) disclaim responsibility for any injury to people or property resulting from any ideas, methods, instructions or products referred to in the content.